
CL-POLYP: A CONTRASTIVE LEARNING-ENHANCED NETWORK FOR ACCURATE POLYP SEGMENTATION

Desheng Li, Chaoliang Liu

School of Artificial Intelligence and Computer Science
Jiangnan University
Wuxi, 214122, China.

Zhiyong Xiao*

School of Artificial Intelligence and Computer Science
Jiangnan University
Wuxi, 214122, China.
zhiyong.xiao@jiangnan.edu.cn

ABSTRACT

Accurate segmentation of polyps from colonoscopy images is crucial for the early diagnosis and treatment of colorectal cancer. Most existing deep learning-based polyp segmentation methods adopt an Encoder-Decoder architecture, and some utilize multi-task frameworks that incorporate auxiliary tasks such as classification to enhance segmentation performance. However, these approaches often require additional labeled data and rely on task similarity, which can limit their generalizability. To address these challenges, we propose CL-Polyp, a contrastive learning-enhanced polyp segmentation network. Our method leverages contrastive learning to improve the encoder's ability to extract discriminative features by contrasting positive and negative sample pairs derived from polyp images. This self-supervised strategy enhances visual representation without requiring additional annotations. In addition, we introduce two lightweight and effective modules: the Modified Atrous Spatial Pyramid Pooling (MASPP) module for better multi-scale feature fusion, and the Channel Concatenate and Element Add (CA) module to fuse low-level and upsampled features for improved boundary reconstruction. Extensive experiments on five benchmark datasets—Kvasir-SEG, CVC-ClinicDB, CVC-ColonDB, CVC-300, and ETIS—demonstrate that CL-Polyp consistently outperforms state-of-the-art methods. Specifically, it improves the IoU metric by 0.011 and 0.020 on the Kvasir-SEG and CVC-ClinicDB datasets, respectively, validating its effectiveness in clinical polyp segmentation tasks.

Keywords Medical Image Segmentation · Polyp Segmentation · Colonoscopy · Contrastive Learning

1 Introduction

Colorectal cancer (CRC) is the third most common cancer globally, with a high incidence of colorectal adenomatous polyps being the primary manifestation[1]. In clinical practice, colonoscopy is the gold standard for identifying diseased tissues in the gastrointestinal tract. Accurate segmentation of polyps from colonoscopy images can provide essential information for treating colorectal cancer.

With the continuous development of the field of computer vision, the method of image semantic segmentation is widely used in polyp segmentation, which simplifies the tedious work of clinicians. In addition, it can better assist medical image analysis and provide more valuable information for clinical practice and pathological research.

Polyp segmentation is also a challenging medical image segmentation task, mainly due to the characteristics of colonoscopy, gastrointestinal tract, and polyps[2]. It mainly includes: 1. Irregular size and shape of polyps; 2. The color of polyps is similar to that of the surrounding intestine, so it is difficult to divide polyps from surrounding mucosa or even residual digestive matter, which also leads to the difficulty of separating the edges of polyps. 3. Polyp segmentation datasets are often small due to the high cost of manual annotation. Existing deep learning methods are gradually solving these problems.

Recently, polyp segmentation methods that use CNN and/or Transformer and mainly adopt the architecture of Encoder-Decoder have achieved great success. The Encoder-Decoder architecture has been widely used in medical image

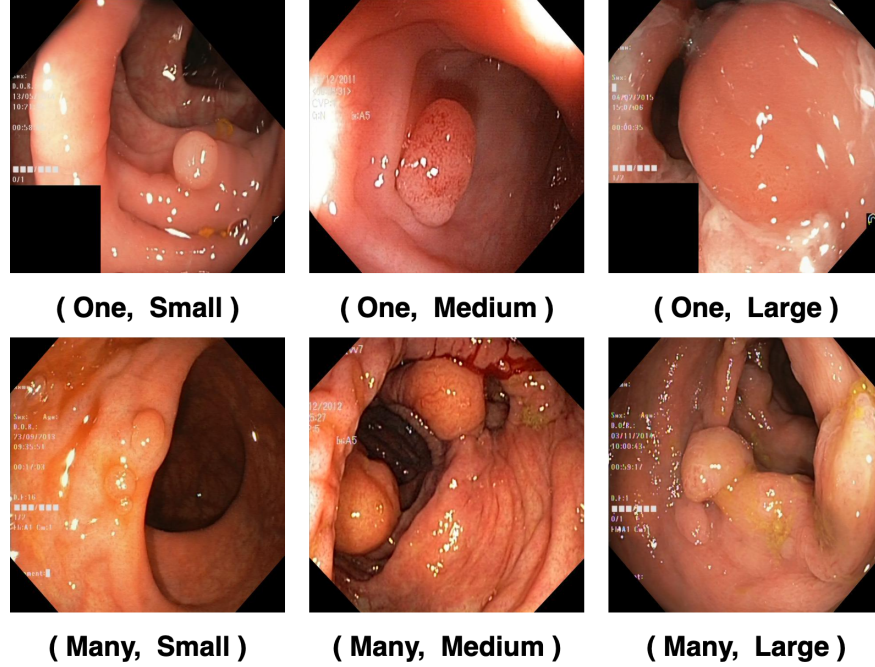


Figure 1: Polyp images from the Kvasir-SEG dataset[3], shown according to the classification method of TGA-Net[4].

segmentation since U-Net, and almost all polyp segmentation methods use this structure. To make it easier to understand, we divide such Encoder-Decoder architectures into three types according to the emphasis of the model structure (or the relative complexity of the Encoder and Decoder).

Architecture with equal emphasis on Encoder and Decoder, such as U-Net[5], U-Net++[6], and ResU-Net ++[7] with a U-shaped structure, usually under the Encoder and Decoder, uses a similar design. It transmits the features of different Encoder layers to Decoder through skip connection, generally using element addition or channel concatenation. The information obtained from the various layers of the encoder is as crucial as the information recovered from the decoder. This paper presents a constrained nonnegative matrix factorization (NMF)-based method for hyperspectral image dimensionality reduction [8].

But more models focus on the structure of the decoder, usually using pre-trained Backbone as the encoder to extract features, but typically pay more attention to skip connections and decoder to improve the boundary information of polyps. It is used to recover the boundary information of polyps, such as Psi-net[9], PraNet[10], SA-Net[11], LDNet[12], and other structures.

Focusing on the structure of the encoder, the design of CNN and/or Transformer is usually used to extract features, and the simple form of the decoder is used to recover detailed information.. Such as DeepLabV3+ [13], TransFuse [14], and Polyp-Pvt [15]. I think the focus of the model is the extraction of Encoder features. DeepLabV3+ uses ResNet [16] to extract features. Polyp-Pvt uses PvT[17] to extract features. TransFuse uses CNN and Transformer as Encoder to obtain better features.

Recently, the structure of the multi-task model has come into our vision[18]. In the Encoder-Decoder structure, more branches are used to do other tasks, and the most commonly used are classification tasks, such as FCP-Net [19] and TGA-Net[4]. In addition to the segmentation task and classification task, FCPNet also has the interaction task of classification and segmentation. TGA-Net classifies polyps according to number and size to optimize Decoder(as shown in Fig.1). The primary role of the multi-task model is to optimize the Encoder through multiple tasks to obtain better features. However, the problem with this is that other functions in the multi-task may not be more effective for the Encoder. The classification task is too single and too specific, and simple classification will not produce good results for segmentation [20]. since multi-task models usually require additional label information, such as classifying benign and malignant tumors, it requires more manually annotated information and increases the workload of medical staff [21].

In order to improve the accuracy and robustness of medical image segmentation, a medical image segmentation method based on improved convolutional neural network is proposed [22]. A deep learning-based method called SR-Net combines a bidirectional recurrent convolutional network (S-Net) for inter-slice correlation and a refinement network (R-

Net) for intra-slice detail enhancement, along with deformable convolutions and data consistency operations, to improve the quality and speed of undersampled multislice MR image reconstruction [23]. This paper proposes a lightweight multi-view hierarchical split network (MVHS-Net) for brain tumor segmentation in MRI images, which achieves high accuracy with significantly reduced computational complexity compared to existing methods [24]. This paper proposes a lightweight CNN-MLP hybrid model called RMMLP, which uses rolling tensors and matrix decomposition to effectively capture local and global features for accurate skin lesion segmentation, achieving state-of-the-art results with fewer parameters compared to Transformer-based methods [25]. This paper proposes a novel semi-supervised medical image segmentation method that integrates a dual-teacher architecture—combining CNN and Transformer models—with uncertainty-guided training to effectively leverage both labeled and unlabeled MRI data, achieving superior segmentation performance using limited annotations [26]. This paper proposes a lightweight 3D hippocampus segmentation method called Light3DHS, which combines a multi-scale convolutional attention module and a 3D MobileViT block to effectively fuse local and global features, achieving superior segmentation performance with fewer parameters and lower computational cost on multiple public datasets [27].

As the demand for early diagnosis and treatment of colorectal cancer increases, the accuracy of polyp segmentation becomes particularly important. Currently, traditional deep learning methods have achieved some success in segmentation tasks, but they still face challenges such as small dataset sizes, high annotation costs, and the diverse shapes of polyps. These factors make it difficult for models to achieve ideal performance in practical applications. Therefore, exploring new learning methods to enhance segmentation accuracy, especially through contrastive learning to improve the model’s sensitivity to polyp features, has become a key motivation for this research. To address the above challenges, we propose adding a contrastive learning-related visual representation learning task in training the polyp segmentation model, called CL-Polyp. Contrastive learning is a self-supervised learning approach that emphasizes learning representations by contrasting positive and negative pairs. In the context of polyp segmentation, contrastive learning can enhance the model’s ability to discern subtle differences between polyp and non-polyp regions. By maximizing the similarity between positive samples—such as different views or augmentations of the same polyp—and minimizing the similarity between negative samples, the model can develop a more robust feature representation. This capability is particularly beneficial in medical imaging, where variability in polyp appearance can complicate segmentation tasks. Specifically, we add a contrastive learning task to the polyp segmentation network. According to the classification standards of the number and size of polyps in TGANet, Positive and negative samples for the contrastive learning task are selected and subjected to reasonable data augmentation. The polyp image is passed through the encoder to extract semantic information, and the encoder with momentum update is used to extract the information of positive and negative sample pairs. The whole Encoder-Decoder model is optimized by optimizing the loss function of contrastive learning and the segmentation loss function.

CL-Polyp is similar to the multi-task segmentation model but different from the specific multi-task model, the model can implicitly learn features to optimize the segmentation results through contrastive learning, and better visual representation can be obtained. In addition, to better use the features in Encoder, we also modify the SOTA model DeepLabV3+. We propose the MASPP module, which can better fuse the deep multi-scale features. For recovering polyp boundary information, we presented the channel Concat and element Add (CA module) to make a better fusion between the low-level feature and upsampling feature, which can reconstruct the polyps’ boundary information. Finally, we validate our model on five challenging polyp segmentation datasets: Kvasir-SEG, CVC-ClinicDB, CVCColonDB, CVC-300, and ETIS. Specifically, on the Kvasir-SEG dataset, our method can achieve a mean Dice of 0.918 and an IoU of 0.864. On the CVC-ClinicDB dataset, our approach can perform a mean Dice of 0.955 and an IoU of 0.915.

To summarize, the main contributions of this paper are as follows:

- We propose a novel polyp segmentation framework that incorporates contrastive learning to optimize the encoder. Unlike traditional multi-task models, our approach improves feature representation without requiring additional annotation, enhancing the encoder’s learning capability in a self-supervised manner.
- We design two lightweight yet effective modules to improve segmentation performance: the Modified Atrous Spatial Pyramid Pooling (MASPP) module for enhanced multi-scale feature fusion, and the Channel Concatenate and Element Add (CA) module for efficient integration of low-level and upsampled features.
- Extensive experiments conducted on five challenging polyp segmentation datasets demonstrate that our method outperforms existing state-of-the-art approaches in both accuracy and robustness.

Next, in Section 2, we will briefly introduce the related work in the form of Fig.1. Then, we introduce our primary method in detail in Section 3, and the experimental session is in Section 4. Finally, we make a conclusion and future work in Section 5.

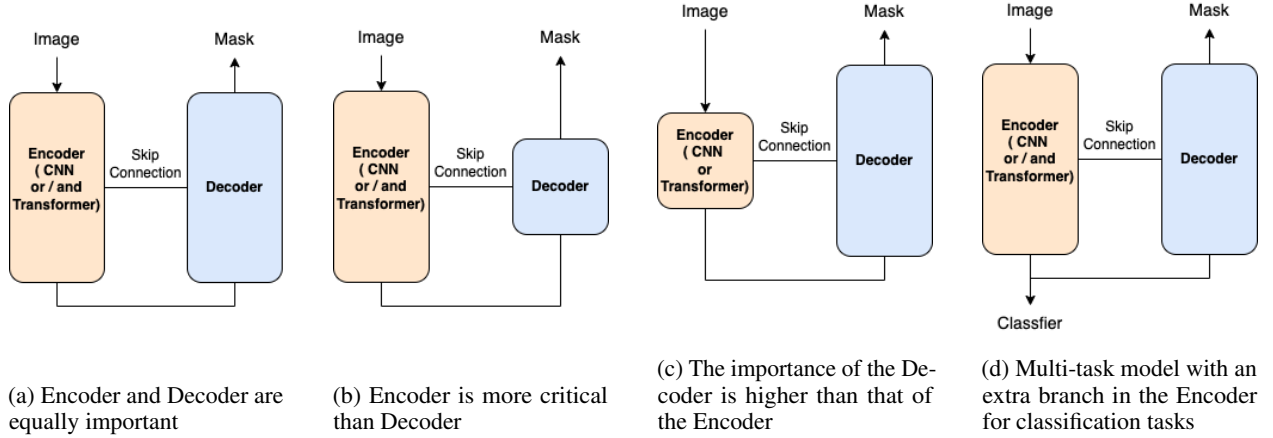


Figure 2: The Encoder-Decoder structure of the polyp segmentation model usually consists of three parts: Encoder, Decoder, and Skip Connection. The relative sizes of the Encoder and Decoder are expressed as structural emphasis or relative complexity. Graph a shows that Encoder and Decoder are equally important; Graph b shows that Encoder is more critical than Decoder; Graph c shows that the importance of the Decoder is higher than that of the Encoder; Graph d shows the multi-task model. The simple form of the model is to have an extra branch in the Encoder for classification tasks.

2 Related work

2.1 Polyp segmentation

In recent years, more segmentation methods based on deep learning have been proposed with broad applications and further development of deep learning. FCN[28] is the first architecture to implement semantic segmentation end-to-end. The proposed U-Net[5] is a U-shaped symmetric method that uses an Encoder-Decoder structure and recovers image segmentation details through skip connections. This simple and effective structure is widely used in medical image segmentation. Based on this method, many researchers have optimized on top of this benchmark method. We classify the structure of such encoder-decoders by the criteria of Encoder-Decoder relative size expressed as structural emphasis and/or relative complexity(As shown in Fig.2). The Encoder-Decoder architecture includes an Encoder to generate feature maps and obtain high-level semantic information, a Decoder to recover spatial information, and a Skip Connection to fuse low-level and high-level features to improve segmentation details(think of the structure of the skip connection as a part of the Decoder).

1.The structure with equal emphasis on Encoder and Decoder is shown in Fig.2a. FCN, U-Net, U-Net++[6], and ResU-net++[7] belong to this type of structure. U-Net++ proposes dense skip connections and explores the effect of the multi-layer U-Net structure. ResU-Net++ uses four techniques to optimize the segmentation network, which are residual calculation, squeeze and excitation[29], atrous spatial pyramidal pooling[13], and attention mechanism[30].

2.The structure of the model focused on Encoder is shown in Fig.2b. This type of structure focuses on extracting features through the Encoder, but this does not mean that the Decoder is not essential; the Decoder is still a vital part. The Encoder uses the architecture of CNN and/or Transformer. The Transformer is supposed to be able to establish long-distance dependencies due to this property the Transformer. Encoders using transformers tend to obtain more valuable and robust features, but this approach increases computation due to how MSA is calculated. Some models use the Transformer structure as the Encoder to get better features, and through the fusion module, the features between the high and low layers are fused.

DeepLabV3+[13], Polyp-Pvt[15], HarDNet-MSEG[31], and TransFuse[14] belong to this class of structures. The DeepLabV3+ model uses ResNet[16] as the Encoder model and uses the atrous convolution ASPP module to achieve the best effect on natural image semantic segmentation using only two upsampling. The HarDNet-MSEG model uses the HarDBlk module as the Encoder, which can get features Polyp-pvt and TransFuse differ from DeepLabV3+, and it uses the structure of a Transformer as Encoder. Polyp-Pvt uses Pvt[17] as Encoder and proposes a cascaded feature fusion module in Decoder, which achieves good results. TransFuse combines CNN and Transformer as the Encoder to extract spatial information and context dependencies.

3. The structure of the model focused on Decoder is shown in Fig.2c. This kind of structure usually uses the existing Backbone structure to extract features. Still, the focus of the structure is on the Decoder part. Compared with other models, the model focusing on the Decoder is the most. PraNet[10], SA-Net[11], MSNet[32], CaraNet[33] and GLFRNet[34] belong to this category. PraNet uses Res2Net[35] as Encoder, adds an inverted attention module to the Decoder, and combines deep supervision to focus on the boundary area of polyps, which has a good effect. SA-Net adds shadow attention in the Decoder to improve the effect of small polyps. In addition, it proposes color exchange data enhancement to solve a certain over-fitting problem. BoxPolyp[36] uses SA-Net as the baseline model and utilizes the bounding box utilization of a larger dataset, and solves a certain over-fitting problem by combining the bounding box with the model results. MSNet added MS Module in skip connection and Decoder, with multi-level and multi-stage cascaded subtraction operations, the complementary information from lower order to higher order among different levels can be effectively obtained. GLFRNet focuses on the process of skip connection and Decoder. The GFR module expands the receptive field and enriches the low-level semantic information. Then the LFR module is used for upsampling and feature fusion. A semi-supervised CT image segmentation method combines CNN and Transformer using entropy-constrained contrastive learning, which can improve segmentation accuracy by filtering unreliable pseudo-labels and leveraging both local and global feature information [37].

Some lightweight structures also belong to Fig.2c. Such as FRCNet[38]. FRCnet proposes the ECC module and the PCF module. The simple CNN structure was used as the Encoder, ECC module was added to the Decoder to fuse the fusion between up-sampling, and PCF was used for context fusion.

2.2 Multi-task model

Multi-task learning is a method to improve the learning ability of an encoder by learning tasks in parallel. In medical image segmentation, the relatively common segmentation task is combined with the classification task as shown in Fig.2d. The primary purpose of this structure is to obtain better segmentation results through multi-task learning. CVNet[39] uses the classification task to optimize the segmentation task in 3D chest ultrasound image segmentation to classify tumors into benign and malignant to optimize the learning ability of the Encoder. FCPNet[19] proposes a task of feature compression pyramid network guided by game-theoretic interactions to conduct the segmentation task together with the classification task. Recently, TGANet[4] divided polyps into three categories according to number and size, one and multiple according to number, and small, medium and large according to size, and used the information obtained by classification as text attention guidance for segmentation.

Multi-task learning can enhance the Encoder without making many modifications to the model and without increasing the computational load of the model. However, the disadvantage of multi-task models is that other tasks have specific results, which may need to be more effective for segmentation. If not, it may even have the opposite effect. At the same time, it requires more label information, which increases the workload of medical staff.

2.3 Contrastive learning

Contrastive learning is the ability to learn generalization and transfer from unlabeled data. The general method is to construct positive and negative samples for each data sample, and the core is to shorten the distance from the positive sample. At the same time, the distance between negative samples is increased. In this process, the selection of negative samples is the most important. MoCo[40] uses dynamic memory to store negative samples in momentum encoder storage. SimCLR[41] shows that large batch sizes as well as long training times are also important for contrastive learning. By introducing a stopping gradient, SimSiam[42] indicates that meaningful representations can be learned from simple network architectures without negative pairs, large batch sizes, or momentum encoders. Few researchers have used contrastive learning in polyp segmentation models, although this method is very effective.

3 Methods

In this paper, we propose that CL-Polyp consists of two branches: the segmentation and the contrastive learning branches. The main branch is the polyp segmentation branch, and the addition of contrastive learning is the auxiliary. The implementation details are provided below.

3.1 Contrastive learning branch

3.1.1 Selection of positive and negative samples

The training by contrastive learning is similar to the training method of the multi-task model structure, which uses a mixed loss function to train the network structure. Contrastive learning focuses on constructing positive and negative

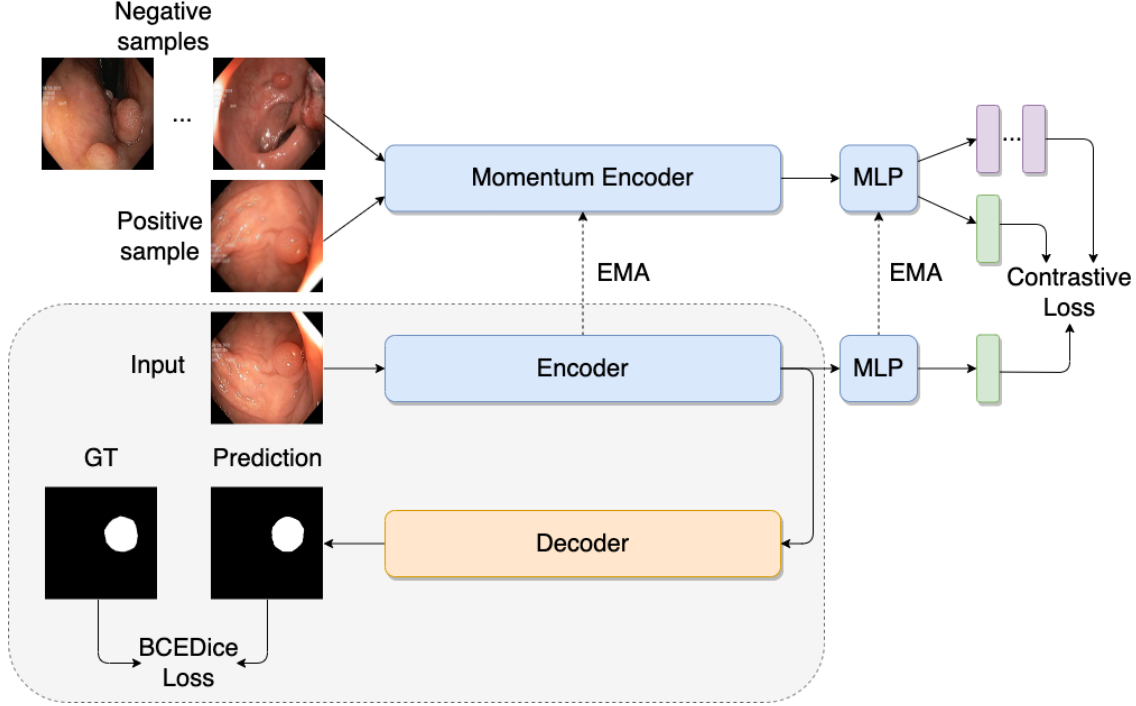


Figure 3: A ResNet50 Encoder extracts the feature map of an image and then enters it into two branches. One branch is used for the segmentation task. The other branch is compared with the features obtained by the momentum updating Encoder with positive and negative samples. The MLP of the contrast learning branch is composed of the Linear layer, BN layer, ReLU layer, and Linear layer. The grey box part represents the inference process.

sample pairs for data. In this paper, according to the classification method of data in TGANet[4], polyps are divided into one or more according to the number of polyps and the size. According to the number of polyps, the data can be divided into one or many; According to the size of polyps, they can be classified into small, medium, and large. Combining the number and size categories, the total can be divided into six categories, as shown in Fig.1.

N and S respectively, polyp number and size of the collection, polyp size, and the number of data sets described as polyps set $C = N \times S = \{(n, s) | n \in N, s \in S\}$. Training set data $D_{tr} = \{(x, c) | c \in C\}$. Through this division, it is very convenient to select positive and negative samples.

Let's consider specific data for D_{tr} a data of x^i , for the description of the sample for $c = \{(n, s) | n = \hat{n}, s = \hat{s}\}$. The number of polyps in the image can be represented as \hat{n} , and the size can be represented as \hat{s} . The description of the sample for $c = \{(n, s) | n = \hat{n}, s = \hat{s}\}$.

There are two ways to select positive samples x_p^i similar to the original image, one is data augmentation of image and the other is from $c = \{(n, s) | n = \hat{n}, s = \hat{s}\}$ choose one of the data as the positive example. In our experiments, we choose one kind of data augmentation of the image as the positive sample. The number and size of polyps in the positive sample are the same as in this data. Negative selection and the image size and the number of samples of different samples, the samples of negative samples x_n^i to choose $\{(n, s) | n \neq \hat{n}, s \neq \hat{s}\}$.

3.1.2 Detailed structure

As shown in Fig.3, the Encoder comprises a ResNet and an MLP. Specifically, ResNet50 is used. The MLP consists of a Linear layer, BN layer, ReLU activation function, and Linear layer. The image passes through the last layer block of ResNet, after which it is divided into two branches, one branch is used for contrastive learning, and the other branch enters the main segmentation branch. After average pooling, the branch features of contrastive learning obtain 2048 dimensional vector features and, finally, 2048 dimensional vector features after MLP. Specifically, x^i extracted the visual features h of the polyp image through the Encoder, x_p^i, x_n^i respectively by a momentum encoder of the same structure through the structure respectively after obtaining h_p, h_n . The parameters of the momentum encoder are updated utilizing momentum in the following way.

$$\theta_k = m\theta_k + (1 - m)\theta_q \quad (1)$$

Then we use contrastive learning loss function to optimize these three feature vectors. The overall training process is presented in Algorithm.1. For the inference procedure, as shown in the gray box in Fig.3, there are no positive and negative samples and the process of momentum Encoder.

Algorithm 1 Pseudo code for the training procedure of CL-Polyp in a PyTorch-like style

Input: input data x^i , K negative samples x_n^i
Output: segmentation prediction
Initialize F_q, F_k : encoder networks for query and key
Initialize D : decoder network
 $F_k.params = F_q.params$
for $x, GT, K * x_n$ in loader **do**
 $x_q, x_p, x_n = \text{aug}(x), \text{aug}(x), \text{aug}(x_n)$
 $h, h_p, h_n = f_q.forward(x_q), f_k.forward(x_p), f_k.forward(x_n)$
 for i in K **do**
 loss += $L_{CL}(h, h_p, h_n)$
 end for
 prediction = $D.forward(h)$
 loss += $L_{SEG}(GT, \text{prediction})$
 loss.backward()
 update($F_q.params, D.params$)
 $F_k.params = m * F_k.params + (1 - m) * F_q.params$
end for

3.1.3 Contrastive Learning Loss Function

The contrastive learning method ensures that the features of a polyp image X^i are similar to the positive sample X_p^i , and For image features, the distance between image features and positive features is always closer than the distance between features of negative samples and image features. The loss function of contrastive learning is introduced to optimize h, h_p , and h_n to reduce the distance between h and h_p . At the same time, the distance between h , and each negative sample h_n is increased. The triplet loss function is adopted, which is proposed in Face-Net[43] and the specific loss function can be described as

$$L_{CL} = \sum_{i=1}^N [\|f(x^i) - f(x_p^i)\|_2^2 - \|f(x^i) - f(x_n^i)\|_2^2 + \alpha] \quad (2)$$

Where α is the interval between positive and negative samples. N is all instances of the training set. In the actual algorithm, one image data corresponds to one positive sample and K negative samples. In my experiment, K is set to 4.

3.1.4 Choices for data augmentation

Learning data invariance is crucial for contrastive learning[44]. Proper selection of data augmentation is essential for understanding data invariance, which directly impacts the model's learning ability. In polyp segmentation tasks, common data augmentation methods include image resizing and cropping, rotation, horizontal flipping, color transformation, and grayscale change. However, we selected random cropping, resizing, rotation, horizontal flipping, Gaussian noise, and normalization as our data augmentation techniques.

3.2 Segmentation branch

Unlike other models focusing on Decoder[45], we adopt the DeepLabV3+ network structure as the Baseline model. Although the Baseline segmentation results are excellent, some things could still be improved so that we can achieve good results with only a few simple modifications to the Baseline model. We propose an enhanced ASPP module named MASPP module and use the CA module to improve the model. Our model belongs to the model that pays more attention to Encoder, as shown in Fig.2b. Although the Decoder has been modified, the focus is still on the features obtained through the Encoder. The detailed structure of our model can be seen in Fig.4.

3.2.1 Modified ASPP module

The ASPP module proposed in DeepLabV3+, ASPP module can obtain multi-scale information through multiple dilated convolution modules with different proportions. In ASPP, channel concatenates, and 1x1 convolution layers are used to

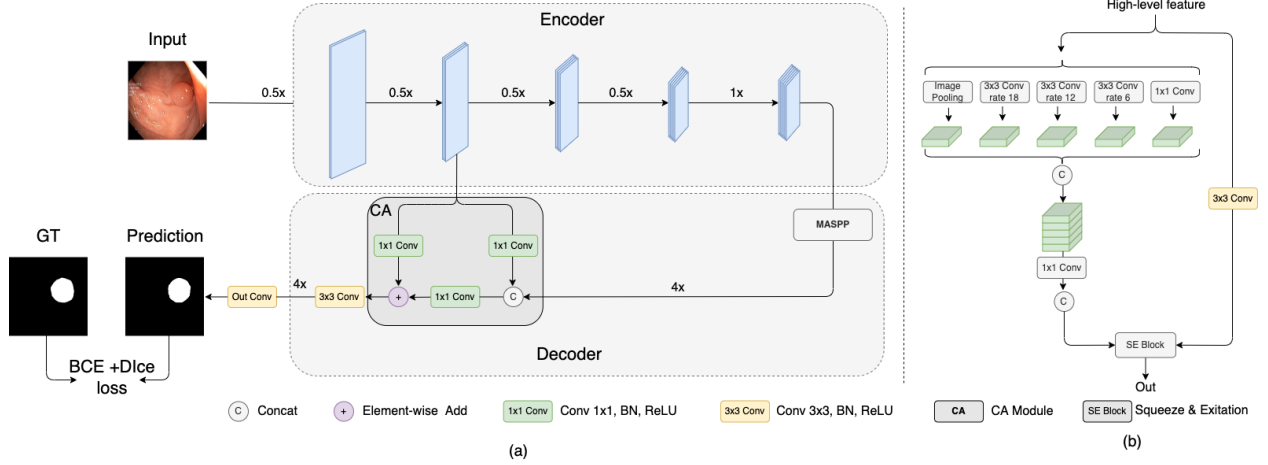


Figure 4: Graph a presents the overall structure of the segmentation model which is the inference procedure of Fig.3. We use ResNet50 as Encoder, in Decoder we use our proposed MASPP module and CA module. Graph b shows the detailed structure of the MASPP module.

fuse multi-scale information after multiple dilated convolutions. Still, the fusion of multi-scale information can only partially be carried out by using channel concatenate. Therefore, we propose a module called Modified Atrous Spatial Pyramid Pooling (MASPP module) which can better fuse high-level multi-scale features.

Fig.4b shows the detailed MASPP module. The high-level feature information f_5 , and then two branch structures, the first branch structure is a ASPP module, after multiple dilated convolution modules, the channel concatenate and 1x1 convolution are simply fused. The other branch structure is to maintain the original feature structure, the features passed through 3x3 convolution layers, BN layers, and ReLU activation layers. After that, an SE module, proposed in SENet[29], is used to fuse these two branch features. The SE module includes Squeeze & Excitation. In the Squeeze module, the first average pooling turn the feature $f_5 \in \mathbb{R}^{C \times H \times W}$ into a shape of $C \times 1 \times 1$. Then through a Linear layer, the ReLU activation layer, Linear layer becomes a shape of $H \times W \times 1 \times 1$ and then the original data and the activated vector are multiplied, which can better fuse multiple features. This can be expressed as follows.

$$f = \text{SE}(\text{Conv}(f_5), \text{ASPP}(f_5)) \quad (3)$$

3.2.2 Using the CA module

In Deeplabv3+ model, skip connection improves the boundary information of the second layer features in Decoder. While using only one layer of features is great, this ignores features from other layers. We propose the CA module to better fuse the features into the Decoder. The second layer feature $f_2 \in \mathbb{R}^{C \times H \times W}$, l represents the second number of layers of the feature, after two 1 x 1 convolution will output two features A_i, B_i , and the upsample feature z_i , concrete can be expressed as $z_i = A_i + \text{Conv}(\text{cat}(B_i, z_i))$. A 4-fold upsampling operation and an Outconv then obtain the final prediction result.

3.2.3 Segmentation branch loss function

To reduce overfitting, we adopt the BCEDice loss used in nnU-Net[46]. It consists of Dice loss, and BCE loss. Dice loss can be widely applied to medical image tasks and is written as follows.

$$L_{Dice} = 1 - 2 \times \frac{\sum_i P_i G_i}{\sum_i P_i + \sum_i G_i} \quad (4)$$

BCE loss can be understood as follows.

$$L_{BCE} = - \sum_i [(1 - G_i) \ln(1 - P_i) + G_i \ln(P_i)] \quad (5)$$

Where i denotes the index of all pixels in the probability distribution map. P_i is the probability that the i -th pixel belongs to the segmented region, and G_i is the true value of the i -th pixel. Finally, the loss function of the segmentation part consists of two parts: BCEloss and Dicoloss.

$$L_{Seg} = L_{BCE} + L_{Dice} \quad (6)$$

3.3 Hybrid loss function

The overall loss function consists of two parts: the loss function of contrastive learning and the loss function of segmentation.

$$L_{Total} = L_{Seg} + \beta L_{CL} \quad (7)$$

Where β is the hyper-parameter and is set to 0.5 in our experiments.

4 Experiment

4.1 Datasets and Experiment Scenarios

To verify the effectiveness and accuracy of our method, we mainly use five datasets commonly used in polyp segmentation, which are respectively Kvasir-SEG[3], CVC-ClinicDB[47], CVC-ColonDB[48], CVC-300[49] and ETIS[50].

The Kvasir-SEG dataset consists of 1000 images. The images in the dataset are irregular in size, ranging from 332x487 to 1920x1072. The size of the polyp ranged from 0.79 % to 62.13 %, and the shape and size of the polyp were irregular. So it's the most challenging. The CVC-ClinicDB dataset includes 612 images obtained from 29 polyp videos. The image size is 384 x 288. The size varies from 0.34% to 45.88%. The CVC-ColonDB dataset includes 380 images obtained from 16 colonoscopy videos with an image size of 574 x 500. Polyp size from 0.30% to 63.15 %. The CVC300 dataset is a cross-domain dataset that contains 60 polyp images. The ETIS dataset includes 196 images obtained from 16 enteroscopy videos. The image size is 1225 x 996. It has a larger resolution compared to other images.

Experiment Scenario I: Our experiments on the Kvasir-SEG dataset alone. We split it into 700/300 for training and test sets instead of 800/100. The reason for the separate experiment is that the sample size of Kvasir-SEG is the most significant and more complex compared to other datasets. The experimental results of our method on this data set can reflect the learning ability of the method.

Experiment Scenario II: We train according to the method of PraNet. PraNet is an extensive training exercise designed to test the generalization performance of a method. Images from Kvasir-SEG and CVC-ClinicDB were randomly divided into 90% for training and 10% for testing. The training set contains 1450 images (900 Kvasir-SEG images and 550 CVC-ClinicDB images are 90% randomly split from their respective datasets). The remaining data from Kvasir-SEG, CVC-ClinicDB, CVC-ColonDB, CVC300, and ETIS datasets were used for testing, which was used to evaluate the generalization ability of the model.

Experiment Scenario III: We conduct ablation experiments on the Kvasir-SEG dataset. To verify the effectiveness of the various modules proposed in our method, the training set and test set are divided in the same way as that of Experiment Scenario I. Ablation experiments on the Kvasir-SEG dataset can reveal the effectiveness of each part of our method. In addition, we conducted experiments to verify the impact of different data augmentations on the model.

4.2 Experiment settings

The experiments use the PyTorch framework on Ubuntu22.04, using python version 3.9. The hardware device, using a single NVIDIA 1080TI GPU with 11GB memory, accelerates our segmentation model's training with a mini-batch size of 4. Using the Adam optimizer, the model used an initial learning rate of 1e-4 to train our model. Learning Rate Decay Strategy Cosine learning rate decay strategy is chosen. Besides, the input images are resized to 384 x 384. Due to reasons with our training method, we trained 300 epochs for both Experiments Scenario I, Experiment Scenario II, and Experiment Scenario III.

4.3 Evaluation metrics

The most common medical image segmentation task uses the Dice coefficient and IoU as evaluation indicators. Most models use this to evaluate how good the model is. We used Dice and IoU as evaluation indexes in Experimental Scenario I, II, and III. The dice coefficient is a standard measure to compare the predicted label with the actual value. It can be defined as:

$$Dice = \frac{2 \times TP}{2 \times TP + FP + FN} \quad (8)$$

IoU is another standard segmentation evaluation measure used to calculate the overlap between the predicted and true values. According to the following formula definition:

$$IoU = \frac{TP}{TP + FP + FN} \quad (9)$$

Table 1: Experiment Scenario I: Results of ten medical image segmentation methods on the Kvasir-SEG dataset.

Method	Kvasir-SEG				
	Dice	Iou	Precision	Recall	F2
U-Net(MICCAI’15)	0.826	0.747	0.870	0.850	0.835
U-Net++(TMI’19)	0.830	0.753	0.863	0.834	0.833
DeepLabV3+(ECCV’18)	0.889	0.827	0.912	0.906	0.898
PraNet(MICCAI’20)	0.894	0.830	0.913	0.906	0.898
HarDNet-MSEG(arXiv)	0.904	0.848	0.907	0.923	0.915
TransFuse-S(MICCAI’21)	0.901	0.839	0.913	0.905	0.906
TransFuse-L(MICCAI’21)	0.902	0.844	0.914	0.905	0.906
TGANet(MICCAI’22)	0.898	0.833	0.912	0.913	0.903
GLFRNet(TMI’22)	0.911	0.853	0.927	0.900	0.913
CL-Polyp(Ours)	0.918	0.864	0.946	0.910	0.915

TP, FP, TN, and FN represent True Positive, False Positive, True Negative, and False Negative respectively. In addition, we also compared three indexes, namely precision, recall, and F2 score in Experiment Scenario I.

$$precision = \frac{TP}{TP + FP} \quad (10)$$

$$recall = \frac{TP}{TP + FN} \quad (11)$$

$$F2 = \frac{5 \times Precision \times Recall}{4 \times Precision + Recall} \quad (12)$$

4.4 Experiment result

4.4.1 The result of Experiment Scenario I

In Experiment Scenario I, we compare our CL-Polyp with ten medical image segmentation methods, including U-Net[5], U-Net++[6], DeepLabV3+[13], PraNet[10], HarDNet-MSEG[31], TransFuse-S/L[14], TGANet[4], and GLFRNet[34]. Among them, U-Net, U-Net++ and DeepLabV3+ are classic image segmentation methods; PraNet, HarDNet-MSEG, TransFuse-S/L, TGANet, and GLFRNet are recently advanced polyp segmentation methods.

Table 1 shows the results on the Kvasir-SEG dataset. The comparison of these models all achieved good performance, with Dice above 0.90 and IoU above 0.83. Some methods failed to reach the highest accuracy in the paper, because Experiment Scenario I was only conducted on the Kvasir-SEG dataset. The PraNet method achieved a Dice of 0.894 and IoU of 0.830. The average Dice of TransFuse-S/L was 0.90 and IoU was 0.84. GLFRNet (TMI’22) had the highest Dice of 0.911 and IoU of 0.853. The best result of our proposed method is that Dice reaches 0.918 and IoU reaches 0.864, which is higher than TGANet which uses the same partitioning method as us. Both metrics of our methods Precision and F2 are also the highest.

To show our model intuitively, we provide results of our model on Kvasir-SEG test images and compare testing results with six advanced models. As shown in Fig.5, the proposed method can obtain better outcomes for the input image in the first four rows, regardless of the overall polyp or the edge details. Our approach can distinguish multiple polyps clearly for the figure’s last three rows of pictures, while other models are challenging to determine. Especially for the polyps with fuzzy boundaries in the last row, our method can still effectively segment the polyps.

4.4.2 The results of Experiment Scenario II

In Experiment Scenarios II, we compare our CL-Polyp with ten medical image segmentation methods, including U-Net, U-Net++, PraNet, SA-Net[11], MSNet[32], PolypPvt[15], BoxPolyp-Res2Net[36] and LDNet[12]. Among them, U-Net and U-Net++ are classic image segmentation methods. PraNet, SA-Net, MSNet, PolypPvt, BoxPolyp-Res2Net, and LDNet are recently advanced polyp segmentation methods.

The results are shown in Table 2 and Table 3. Results on Kvasir-SEG and CVC-ClinicDB. As we can see, our proposed model achieves a very high level on both data sets. Specifically, on the Kvasir-SEG dataset, Dice and IoU were 0.917 and 0.864, respectively. Our method performs almost as well as polyp-Pvt using Pvt as the Encoder on the Kvasir-SEG dataset. We performed better in the CVC-ClinicDB dataset, with Dice and IoU reaching 0.955 and 0.915, respectively, exceeding the existing methods LDNet 1.2% and 2%, respectively.

Table 2: Results of 10 medical image segmentation methods on Kvasir-SEG and CVC-ClinicDB datasets by the training method of PraNet.

Method	Kvasir-SEG		CVC-ClinicDB	
	Dice	IoU	Dice	IoU
U-Net(MICCAI'15)	0.818	0.746	0.823	0.750
U-Net++(TMI'19)	0.821	0.743	0.790	0.729
PraNet(MICCAI'20)	0.898	0.840	0.899	0.849
SA-Net(MICCAI'21)	0.904	0.847	0.916	0.859
MSNet(MICCAI'21)	0.905	0.849	0.918	0.869
Polyp-Pvt(arXiv)	0.917	0.864	0.937	0.889
BoxPolyp-Res2Net(MICCAI'22)	0.910	0.857	0.904	0.849
LDNet(MICCAI'22)	0.907	0.853	0.943	0.895
CL-Polyp(Ours)	0.917	0.864	0.955	0.915

Table 3: Results of ten medical image segmentation methods on the CVC-ColonDB, CVC-300 and ETIS datasets by the training method of PraNet. '-' denotes that the corresponding value is not reported.

Method	CVC-ColonDB		CVC-300		ETIS	
	Dice	IoU	Dice	IoU	Dice	IoU
U-Net(MICCAI'15)	0.512	0.444	0.710	0.627	0.398	0.335
U-Net++(TMI'19)	0.483	0.410	0.707	0.627	0.393	0.335
PraNet(MICCAI'20)	0.712	0.640	0.871	0.797	0.628	0.567
SA-Net(MICCAI'21)	0.753	0.670	0.888	0.815	0.750	0.654
MSNet(MICCAI'21)	0.751	0.671	0.865	0.799	0.723	0.652
Polyp-Pvt(arXiv)	0.808	0.727	0.900	0.833	0.787	0.706
BoxPolyp-Res2Net(MICCAI'22)	0.820	0.741	0.903	0.835	0.829	0.742
LDNet(MICCAI'22)	0.784	0.706	-	-	0.744	0.665
CL-Polyp(Ours)	0.770	0.710	0.880	0.812	0.760	0.658

Results on CVC-ColonDB, CVC-300 and ETIS. Our method only used these three data sets for testing, but not for training, to verify the method's generalization ability. It can be seen that although the performance of our approach on these three data sets is also excellent, it fails to reach the optimal index, and there is a gap of about 2 % between our method and the other most advanced methods. This is due to our training method using contrastive learning, through which we can learn good visual representation. Still, to some extent, the model will be trapped in the current data set, which affects the model's generalization ability.

4.4.3 The results of Experiment Scenario III

In this section, we show the necessity of each module in the network in the form of an ablation experiment. We also showed the impact of different data enhancement methods on our approach. We only use the Kvasir-SEG dataset to conduct experiments in this experimental part.

We use the DeepLabV3+ network as our Baseline and verify effectiveness by adding components to Baseline. Baseline + MASPP + CA + CL branch is our final model, CL-Polyp.

Table 4: The comparison of our CL-Polyp with different modules on Kvasir-SEG datasets.

Method	Kvasir-SEG	
	Dice	IoU
Baseline	0.889	0.827
Baseline + MASPP	0.899	0.838
Baseline + MASPP + CA	0.900	0.842
Baseline + MASPP + CA + CL Branch	0.918	0.864

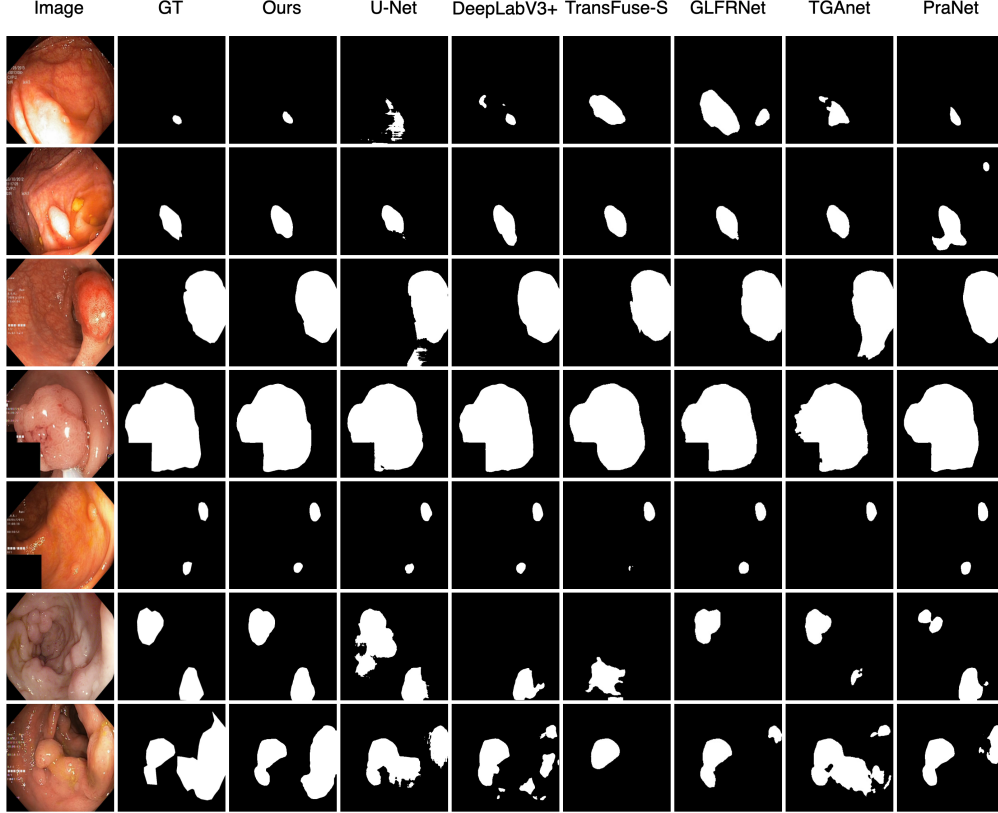


Figure 5: Visual comparison between the proposed method and six state-of-the-art methods.

Table 5: The comparison of our CL-Polyp with different data augmentation on Kvasir-SEG datasets.

Method	Kvasir-SEG	
	Dice	IoU
Base	0.911	0.856
Base + GaussianBlur	0.918	0.864
Base + ToGray	0.903	0.848
Base + BrightnessContrast	0.906	0.851
Base + GaussianBlur + BrightnessContrast	0.910	0.855
Base + GaussianBlur + RandomCrop(0.6 -1.0)	0.909	0.855
Base + GaussianBlur + GridDropout	0.909	0.855

Effectiveness of MASPP Module and CA Module. The results of Baseline + MASPP in Table 4 can demonstrate the effectiveness of the results. After adding the MASPP module, our approach showed a 1.0% and 1.1% improvement in Dice and IoU, respectively. After adding the CA module, our method showed a 0.1% and 0.4% improvement in Dice and IoU, respectively.

Effectiveness of Contrastive learning branch. As shown in Table 4, after adding the CL branch, our approach has a 1.8% and 2.2% increase in Dice and IoU, respectively. This can fully shows that CL Branch has a nice effect.

Effectiveness of different augmentations.

Data enhancement methods are essential for learning data invariance by contrast learning, so we explored the influence of different data enhancement methods on our methods. Table 5 shows the experimental results, where Base data enhancement refers to random resize and crop, and the range of crop is (0.8, 1.0), random rotation, vertical flip, and normalization. Based on base data enhancement, we added gaussian blur, to gray, brightness contrast, and their random

combination and other contents. The ablation results show that only adding the gaussian blur method to the Base data enhancement method can achieve the best results.

References

- [1] Rebecca L. Siegel, Kimberly D. Miller, Ann Goding Sauer, Stacey A. Fedewa, Lynn F. Butterly, Joseph C. Anderson, Andrea Cercek, Robert A. Smith, and Ahmedin Jemal. Colorectal cancer statistics, 2020. *CA: A Cancer Journal for Clinicians*, 70:145–164, 5 2020.
- [2] Shailesh Vitthalrao Bhalerao and Ram Bilas Pachori. Clustering sparse swarm decomposition for automated recognition of upper limb movements from non-homogeneous cross-channel eeg signals. *IEEE Sensors Letters*, 2023.
- [3] Debesh Jha, Pia H. Smedsrud, Michael A. Riegler, Pål Halvorsen, Thomas de Lange, Dag Johansen, and Håvard D. Johansen. Kvasir-seg: A segmented polyp dataset. In Yong Man Ro, Wen-Huang Cheng, Junmo Kim, Wei-Ta Chu, Peng Cui, Jung-Woo Choi, Min-Chun Hu, and Wesley De Neve, editors, *MultiMedia Modeling - 26th International Conference, MMM 2020, Daejeon, South Korea, January 5-8, 2020, Proceedings, Part II*, volume 11962 of *Lecture Notes in Computer Science*, pages 451–462. Springer, 2020.
- [4] Nikhil Kumar Tomar, Debesh Jha, Ulas Bagci, and Sharib Ali. Tganet: Text-guided attention for improved polyp segmentation. In Linwei Wang, Qi Dou, P. Thomas Fletcher, Stefanie Speidel, and Shuo Li, editors, *Medical Image Computing and Computer Assisted Intervention - MICCAI 2022 - 25th International Conference, Singapore, September 18-22, 2022, Proceedings, Part III*, volume 13433 of *Lecture Notes in Computer Science*, pages 151–160. Springer, 2022.
- [5] Olaf Ronneberger, Philipp Fischer, and Thomas Brox. U-net: Convolutional networks for biomedical image segmentation. In Nassir Navab, Joachim Hornegger, William M. Wells III, and Alejandro F. Frangi, editors, *Medical Image Computing and Computer-Assisted Intervention - MICCAI 2015 - 18th International Conference Munich, Germany, October 5 - 9, 2015, Proceedings, Part III*, volume 9351 of *Lecture Notes in Computer Science*, pages 234–241. Springer, 2015.
- [6] Zongwei Zhou, Md Mahfuzur Rahman Siddiquee, Nima Tajbakhsh, and Jianming Liang. Unet++: Redesigning skip connections to exploit multiscale features in image segmentation. *IEEE Trans. Medical Imaging*, 39(6):1856–1867, 2020.
- [7] Debesh Jha, Pia H. Smedsrud, Michael A. Riegler, Dag Johansen, Thomas de Lange, Pål Halvorsen, and Håvard D. Johansen. Resunet++: An advanced architecture for medical image segmentation. In *IEEE International Symposium on Multimedia, ISM 2019, San Diego, CA, USA, December 9-11, 2019*, pages 225–230. IEEE, 2019.
- [8] Zhiyong Xiao and Salah Bourennane. Constrained nonnegative matrix factorization and hyperspectral image dimensionality reduction. *REMOTE SENSING LETTERS*, 5(1):46–54, 2014.
- [9] Balamurali Murugesan, Kaushik Sarveswaran, Sharath M. Shankaranarayana, Keerthi Ram, Jayaraj Joseph, and Mohanasankar Sivaprakasam. Psi-net: Shape and boundary aware joint multi-task deep network for medical image segmentation. In *41st Annual International Conference of the IEEE Engineering in Medicine and Biology Society, EMBC 2019, Berlin, Germany, July 23-27, 2019*, pages 7223–7226. IEEE, 2019.
- [10] Deng-Ping Fan, Ge-Peng Ji, Tao Zhou, Geng Chen, Huazhu Fu, Jianbing Shen, and Ling Shao. Pranet: Parallel reverse attention network for polyp segmentation. In Anne L. Martel, Purang Abolmaesumi, Danail Stoyanov, Diana Mateus, Maria A. Zuluaga, S. Kevin Zhou, Daniel Racoceanu, and Leo Joskowicz, editors, *Medical Image Computing and Computer Assisted Intervention - MICCAI 2020 - 23rd International Conference, Lima, Peru, October 4-8, 2020, Proceedings, Part VI*, volume 12266 of *Lecture Notes in Computer Science*, pages 263–273. Springer, 2020.
- [11] Jun Wei, Yiwen Hu, Ruimao Zhang, Zhen Li, S. Kevin Zhou, and Shuguang Cui. Shallow attention network for polyp segmentation. In Marleen de Bruijne, Philippe C. Cattin, Stéphane Cotin, Nicolas Padoy, Stefanie Speidel, Yefeng Zheng, and Caroline Essert, editors, *Medical Image Computing and Computer Assisted Intervention - MICCAI 2021 - 24th International Conference, Strasbourg, France, September 27 - October 1, 2021, Proceedings, Part I*, volume 12901 of *Lecture Notes in Computer Science*, pages 699–708. Springer, 2021.
- [12] Ruifei Zhang, Peiwen Lai, Xiang Wan, De-Jun Fan, Feng Gao, Xiao-Jian Wu, and Guanbin Li. Lesion-aware dynamic kernel for polyp segmentation. In Linwei Wang, Qi Dou, P. Thomas Fletcher, Stefanie Speidel, and Shuo Li, editors, *Medical Image Computing and Computer Assisted Intervention - MICCAI 2022 - 25th International Conference, Singapore, September 18-22, 2022, Proceedings, Part III*, volume 13433 of *Lecture Notes in Computer Science*, pages 99–109. Springer, 2022.

- [13] Liang-Chieh Chen, Yukun Zhu, George Papandreou, Florian Schroff, and Hartwig Adam. Encoder-decoder with atrous separable convolution for semantic image segmentation. In Vittorio Ferrari, Martial Hebert, Cristian Sminchisescu, and Yair Weiss, editors, *Computer Vision - ECCV 2018 - 15th European Conference, Munich, Germany, September 8-14, 2018, Proceedings, Part VII*, volume 11211 of *Lecture Notes in Computer Science*, pages 833–851. Springer, 2018.
- [14] Yundong Zhang, Huiye Liu, and Qiang Hu. Transfuse: Fusing transformers and cnns for medical image segmentation. In Marleen de Bruijne, Philippe C. Cattin, Stéphane Cotin, Nicolas Padoy, Stefanie Speidel, Yefeng Zheng, and Caroline Essert, editors, *Medical Image Computing and Computer Assisted Intervention - MICCAI 2021 - 24th International Conference, Strasbourg, France, September 27 - October 1, 2021, Proceedings, Part I*, volume 12901 of *Lecture Notes in Computer Science*, pages 14–24. Springer, 2021.
- [15] Bo Dong, Wenhai Wang, Deng-Ping Fan, Jinpeng Li, Huazhu Fu, and Ling Shao. Polyp-pvt: Polyp segmentation with pyramid vision transformers. *CoRR*, abs/2108.06932, 2021.
- [16] Kaiming He, Xiangyu Zhang, Shaoqing Ren, and Jian Sun. Deep residual learning for image recognition. In *2016 IEEE Conference on Computer Vision and Pattern Recognition, CVPR 2016, Las Vegas, NV, USA, June 27-30, 2016*, pages 770–778. IEEE Computer Society, 2016.
- [17] Wenhai Wang, Enze Xie, Xiang Li, Deng-Ping Fan, Kaitao Song, Ding Liang, Tong Lu, Ping Luo, and Ling Shao. Pyramid vision transformer: A versatile backbone for dense prediction without convolutions. In *2021 IEEE/CVF International Conference on Computer Vision, ICCV 2021, Montreal, QC, Canada, October 10-17, 2021*, pages 548–558. IEEE, 2021.
- [18] Shailesh Bhalerao and Ram Bilas Pachori. Essdm: An enhanced sparse swarm decomposition method and its application in multi-class motor imagery-based eeg-bci system. *Authorea Preprints*, 2023.
- [19] Yexin Liu, Jian Zhou, Lizhu Liu, Zhengjia Zhan, Yueqiang Hu, Yongqing Fu, and Huigao Duan. Fcp-net: A feature-compression-pyramid network guided by game-theoretic interactions for medical image segmentation. *IEEE Trans. Medical Imaging*, 41(6):1482–1496, 2022.
- [20] Priyanka Kumar and Shailesh Bhalerao. Detection of tumor in liver using image segmentation and registration technique. *Journal of Electronics and Communication Engineering*, 9(2):110–115, 2014.
- [21] Shailesh Vitthalrao Bhalerao and Ram Bilas Pachori. Imagined speech-eeg detection using multivariate swarm sparse decomposition-based joint time-frequency analysis for intuitive bci. *Authorea Preprints*, 2024.
- [22] Chen Liu, Zhiyong Xiao, and Nianmao Du. Application of improved convolutional neural network in medical image segmentation. *Journal of Frontiers of Computer Science and Technology*, pages 1593–1603, 2019.
- [23] Zhiyong Xiao, Nianmao Du, Jianjun Liu, and Weidong Zhang. Sr-net: A sequence offset fusion net and refine net for undersampled multislice mr image reconstruction. *COMPUTER METHODS AND PROGRAMS IN BIOMEDICINE*, 202, 2021.
- [24] Zhiyong Xiao, Kanghui He, Jianjun Liu, and Weidong Zhang. Multi-view hierarchical split network for brain tumor segmentation. *Biomedical Signal Processing and Control*, 69, 2021.
- [25] Chao Ji, Zhaohong Deng, Yan Ding, Fengsheng Zhou, and Zhiyong Xiao. Rmmlp:rolling mlp and matrix decomposition for skin lesion segmentation. *Biomedical Signal Processing and Control*, 84:104825, 2023.
- [26] Zhiyong Xiao, Yixin Su, Zhaohong Deng, and Weidong Zhang. Efficient combination of cnn and transformer for dual-teacher uncertainty-guided semi-supervised medical image segmentation. *Computer Methods and Programs in Biomedicine*, 226:107099, 2022.
- [27] Zhiyong Xiao, Yuhong Zhang, Zhaohong Deng, and Fei Liu. Light3dhs: A lightweight 3d hippocampus segmentation method using multiscale convolution attention and vision transformer. *NeuroImage*, 292:120608, 2024.
- [28] Jonathan Long, Evan Shelhamer, and Trevor Darrell. Fully convolutional networks for semantic segmentation. In *IEEE Conference on Computer Vision and Pattern Recognition, CVPR 2015, Boston, MA, USA, June 7-12, 2015*, pages 3431–3440. IEEE Computer Society, 2015.
- [29] Jie Hu, Li Shen, and Gang Sun. Squeeze-and-excitation networks. In *2018 IEEE Conference on Computer Vision and Pattern Recognition, CVPR 2018, Salt Lake City, UT, USA, June 18-22, 2018*, pages 7132–7141. Computer Vision Foundation / IEEE Computer Society, 2018.
- [30] Ashish Vaswani, Noam Shazeer, Niki Parmar, Jakob Uszkoreit, Llion Jones, Aidan N. Gomez, Lukasz Kaiser, and Illia Polosukhin. Attention is all you need. In Isabelle Guyon, Ulrike von Luxburg, Samy Bengio, Hanna M. Wallach, Rob Fergus, S. V. N. Vishwanathan, and Roman Garnett, editors, *Advances in Neural Information Processing Systems 30: Annual Conference on Neural Information Processing Systems 2017, December 4-9, 2017, Long Beach, CA, USA*, pages 5998–6008, 2017.

- [31] Chien-Hsiang Huang, Hung-Yu Wu, and Youn-Long Lin. Hardnet-mseg: A simple encoder-decoder polyp segmentation neural network that achieves over 0.9 mean dice and 86 FPS. *CoRR*, abs/2101.07172, 2021.
- [32] Xiaoqi Zhao, Lihe Zhang, and Huchuan Lu. Automatic polyp segmentation via multi-scale subtraction network. In Marleen de Bruijne, Philippe C. Cattin, Stéphane Cotin, Nicolas Padoy, Stefanie Speidel, Yefeng Zheng, and Caroline Essert, editors, *Medical Image Computing and Computer Assisted Intervention - MICCAI 2021 - 24th International Conference, Strasbourg, France, September 27 - October 1, 2021, Proceedings, Part I*, volume 12901 of *Lecture Notes in Computer Science*, pages 120–130. Springer, 2021.
- [33] Ange Lou, Shuyue Guan, and Murray H. Loew. Caranet: Context axial reverse attention network for segmentation of small medical objects. *CoRR*, abs/2108.07368, 2021.
- [34] Jiahuan Song, Xinjian Chen, Qianlong Zhu, Fei Shi, Dehui Xiang, Zhongyue Chen, Ying Fan, Lingjiao Pan, and Weifang Zhu. Global and local feature reconstruction for medical image segmentation. *IEEE Trans. Medical Imaging*, 41(9):2273–2284, 2022.
- [35] Shanghua Gao, Ming-Ming Cheng, Kai Zhao, Xin-Yu Zhang, Ming-Hsuan Yang, and Philip H. S. Torr. Res2net: A new multi-scale backbone architecture. *IEEE Trans. Pattern Anal. Mach. Intell.*, 43(2):652–662, 2021.
- [36] Jun Wei, Yiwen Hu, Guanbin Li, Shuguang Cui, S. Kevin Zhou, and Zhen Li. Boxpolyp: Boost generalized polyp segmentation using extra coarse bounding box annotations. In Linwei Wang, Qi Dou, P. Thomas Fletcher, Stefanie Speidel, and Shuo Li, editors, *Medical Image Computing and Computer Assisted Intervention - MICCAI 2022 - 25th International Conference, Singapore, September 18-22, 2022, Proceedings, Part III*, volume 13433 of *Lecture Notes in Computer Science*, pages 67–77. Springer, 2022.
- [37] Zhiyong Xiao, Hao Sun, and Fei Liu. Semi-supervised ct image segmentation via contrastive learning based on entropy constraints. *Biomedical Engineering Letters*, pages 1023–1035, 2024.
- [38] Liantao Shi, Yufeng Wang, Zhengguo Li, and Wen Qiumiao. Frcnet: Feature refining and context-guided network for efficient polyp segmentation. *Frontiers in Bioengineering and Biotechnology*, 10, 6 2022.
- [39] Yue Zhou, Houjin Chen, Yanfeng Li, Qin Liu, Xuanang Xu, Shu Wang, Pew-Thian Yap, and Dinggang Shen. Multi-task learning for segmentation and classification of tumors in 3d automated breast ultrasound images. *Medical Image Anal.*, 70:101918, 2021.
- [40] Kaiping He, Haoqi Fan, Yuxin Wu, Saining Xie, and Ross B. Girshick. Momentum contrast for unsupervised visual representation learning. In *2020 IEEE/CVF Conference on Computer Vision and Pattern Recognition, CVPR 2020, Seattle, WA, USA, June 13-19, 2020*, pages 9726–9735. Computer Vision Foundation / IEEE, 2020.
- [41] Ting Chen, Simon Kornblith, Mohammad Norouzi, and Geoffrey E. Hinton. A simple framework for contrastive learning of visual representations. In *Proceedings of the 37th International Conference on Machine Learning, ICML 2020, 13-18 July 2020, Virtual Event*, volume 119 of *Proceedings of Machine Learning Research*, pages 1597–1607. PMLR, 2020.
- [42] Xinlei Chen and Kaiping He. Exploring simple siamese representation learning. In *IEEE Conference on Computer Vision and Pattern Recognition, CVPR 2021, virtual, June 19-25, 2021*, pages 15750–15758. Computer Vision Foundation / IEEE, 2021.
- [43] Florian Schroff, Dmitry Kalenichenko, and James Philbin. Facenet: A unified embedding for face recognition and clustering. In *IEEE Conference on Computer Vision and Pattern Recognition, CVPR 2015, Boston, MA, USA, June 7-12, 2015*, pages 815–823. IEEE Computer Society, 2015.
- [44] Shailesh Vitthalrao Bhalerao and Ram Bilas Pachori. Automated classification of cognitive visual objects using multivariate swarm sparse decomposition from multichannel EEG-MEG signals. *IEEE Trans. Hum. Mach. Syst.*, 54(4):455–464, 2024.
- [45] Shailesh Vitthalrao Bhalerao and Ram Bilas Pachori. Sparse spectrum based swarm decomposition for robust nonstationary signal analysis with application to sleep apnea detection from EEG. *Biomed. Signal Process. Control.*, 77:103792, 2022.
- [46] Fabian Isensee, Jens Petersen, André Klein, David Zimmerer, Paul F. Jaeger, Simon Kohl, Jakob Wasserthal, Gregor Köhler, Tobias Norajitra, Sebastian J. Wirkert, and Klaus H. Maier-Hein. nnu-net: Self-adapting framework for u-net-based medical image segmentation. *CoRR*, abs/1809.10486, 2018.
- [47] Jorge Bernal, Francisco Javier Sánchez, Gloria Fernández-Esparrach, Debora Gil, Cristina Rodríguez de Miguel, and Fernando Vilariño. WM-DOVA maps for accurate polyp highlighting in colonoscopy: Validation vs. saliency maps from physicians. *Comput. Medical Imaging Graph.*, 43:99–111, 2015.
- [48] Nima Tajbakhsh, Suryakanth R. Gurudu, and Jianming Liang. Automated polyp detection in colonoscopy videos using shape and context information. *IEEE Trans. Medical Imaging*, 35(2):630–644, 2016.

- [49] David Vázquez, Jorge Bernal, Francisco Javier Sánchez, Gloria Fernández-Esparrach, Antonio M. López, Adriana Romero, Michal Drozdal, and Aaron C. Courville. A benchmark for endoluminal scene segmentation of colonoscopy images. *CoRR*, abs/1612.00799, 2016.
- [50] Juan Silva, Aymeric Histace, Olivier Romain, Xavier Dray, and Bertrand Granado. Toward embedded detection of polyps in WCE images for early diagnosis of colorectal cancer. *Int. J. Comput. Assist. Radiol. Surg.*, 9(2):283–293, 2014.